Characterization and Photoelectrochemical Properties of Nanostructured Thin Film Composed of Carbon Nanohorns Covalently Functionalized with Porphyrins

Georgia Pagona,[†] Atula S. D. Sandanayaka,[‡] Taku Hasobe,*[,‡,§] Georgios Charalambidis,[||] Athanassios G. Coutsolelos,[||] Masako Yudasaka,[#] Sumio Iijima,[#] and Nikos Tagmatarchis*[,†]

Theoretical and Physical Chemistry Institute, National Hellenic Research Foundation, 48 Vass. Constantinou Ave., Athens 116 35, Hellas, School of Materials Science, Japan Advanced Institute of Science and Technology (JAIST), Nomi, Ishikawa 923 1292, Japan, PRESTO, Japan Science and Technology Agency (JST), 4-1-8 Honcho, Kawaguchi, Saitama, 332-0012, Japan, Chemistry Department, Laboratory of Bioinorganic Chemistry, University of Crete, PO Box 2208, Heraklion 710 03, Crete, Hellas, and Fundamental Research Laboratories, NEC Corporation, 34 Miyukigaoka, Tsukuba, Ibaraki 305-8501, Japan

Received: June 18, 2008; Revised Manuscript Received: August 3, 2008

Carbon nanohorns (CNHs) covalently functionalized at the conical tips with porphyrin (H_2P) moieties were used to construct photoelectrochemical solar cells. Electrophoretic deposition was applied to fabricate films of the modified CNHs onto optically transparent electrodes (OTE) while nanostructured SnO_2 films were cast onto the OTE (OTE/SnO_2). The CNH−H_2P film on the nanostructured SnO_2 electrode exhibited an incident photon to current conversion efficiency (IPCE) of 5.8% at an applied bias of +0.2 V vs SCE in a standard three-compartment electrochemical cell. The measured IPCE was found greater than the one observed for the sum of the single components, namely CNHs and H_2P films onto the SnO_2 electrode. Fluorescence lifetime measurements revealed that photoinduced electron transfer from the singlet excited state of the porphyrin to the nanohorns takes place, while direct electron injection from the reduced nanohorns to the conduction band of the SnO_2 electrode occurs. These processes are responsible for the photocurrent generation.

Introduction

Nanometer-sized carbon-based materials such as fullerenes and nanotubes possess enormous potential as integrative components of energy conversion devices because of their unique robustness as well as their novel optical and electrical properties.[1,2] Particularly, the great electron-accepting properties of fullerenes together with the small reorganization energy of electron transfer,[3] leading to a high acceleration of photoinduced charge separation (as well as deceleration of charge recombination), have paved the way toward the construction of some fullerene-based photoelectrochemical devices and solar cells.[4−10] Moreover, in the nanowire-like structure of carbon nanotubes efficient electron and hole transport on electrodes occurs, thus allowing their incorporation into integrative components on photovoltaic and photoelectrochemical devices.[11−16] Recently the photoelectrochemical properties of single-walled carbon nanotubes (SWCNT) as well as of cup-stacked carbon nanotube films cast on conducting glass electrodes have also been reported.[17−19]

Carbon nanohorns (CNH),[20] a nanostructured graphene-based material within the family of SWCNT, are receiving great attention especially because of their unique morphology and unusually high purity. The CNH has a tubular form with a diameter of 2−5 nm and a length of 40−50 nm with a conical end. The CNH form a secondary aggregate having dahlia flower-like spherical morphology with an aggregate diameter of 80−100 nm. The absence of transition metal catalyst during production (i.e., CO_2 laser ablation of a graphite pole, at room temperature under noble gas conditions), greatly differentiates them from conventional carbon nanotubes. In common with carbon nanotubes, CNHs are insoluble in any solvent. However, chemical functionalization of CNHs, resulting in soluble hybrid materials, has been investigated both theoretically[21] and experimentally.[22−25] In this framework, photophysical assays with CNH-based donor−acceptor hybrid materials have been reported. Importantly, these tests provide initial insight into potential applications of CNH in solar energy conversion. Model systems that have been prepared and tested include CNH-based conjugates and hybrids that bear a variety of photosensitizers/electron donors: pyrene,[26] porphyrin,[27−30] ferrocene,[31] and tetrathiafulvalene.[32] These functional building blocks are either covalently attached or interact supramolecularly with the CNH skeleton.

Recently, the covalent attachment of α-5-(2-aminophenyl)-α-15-(2-nitrophenyl)-10,20-bis(2,4,6-trimethylphenyl)porphyrin (H_2P) to CNH via an amide bond was accomplished.[29] Fluorescence quenching and nanosecond transient absorption spectroscopy results indicated that the photoexcited H_2P moieties serve as electron donors, while CNH serve as electron acceptors, resulting in the formation of a charge-separated state $CNH^{\bullet-}-H_2P^{\bullet+}$. Having these results in mind, we investigated the photoelectrochemical behavior of CNH−H_2P fabricated onto an optically transparent electrode (OTE) while nanostructured SnO_2 electrodes were cast onto the OTE. Such light energy conversion systems composed of CNH have yet to be fabricated so far. Herein, the details of the morphology and photoelectrochemical behavior of CNH−H_2P films (OTE/SnO_2/CNH−H_2P) are presented and compared with pristine CNH films (OTE/SnO_2/CNH). In this context, CNH−H_2P is employed as a

* Corresponding authors. (N.T.) Fax: + 30 210 7273794; tel: + 30 210 7273835; e-mail: tagmatar@eie.gr. (T.H.) E-mail: t-hasobe@jaist.ac.jp.
[†] National Hellenic Research Foundation.
[‡] Japan Advanced Institute of Science and Technology (JAIST).
[§] PRESTO.
[||] University of Crete.
[#] NEC Corporation.

10.1021/jp805352y CCC: $40.75
Published on Web 09/13/2008

SCHEME 1: Schematic Illustrations of CNH−H_2P Structure and a Photoelectrochemical Solar Cell of OTE/SnO_2/CNH−H_2P

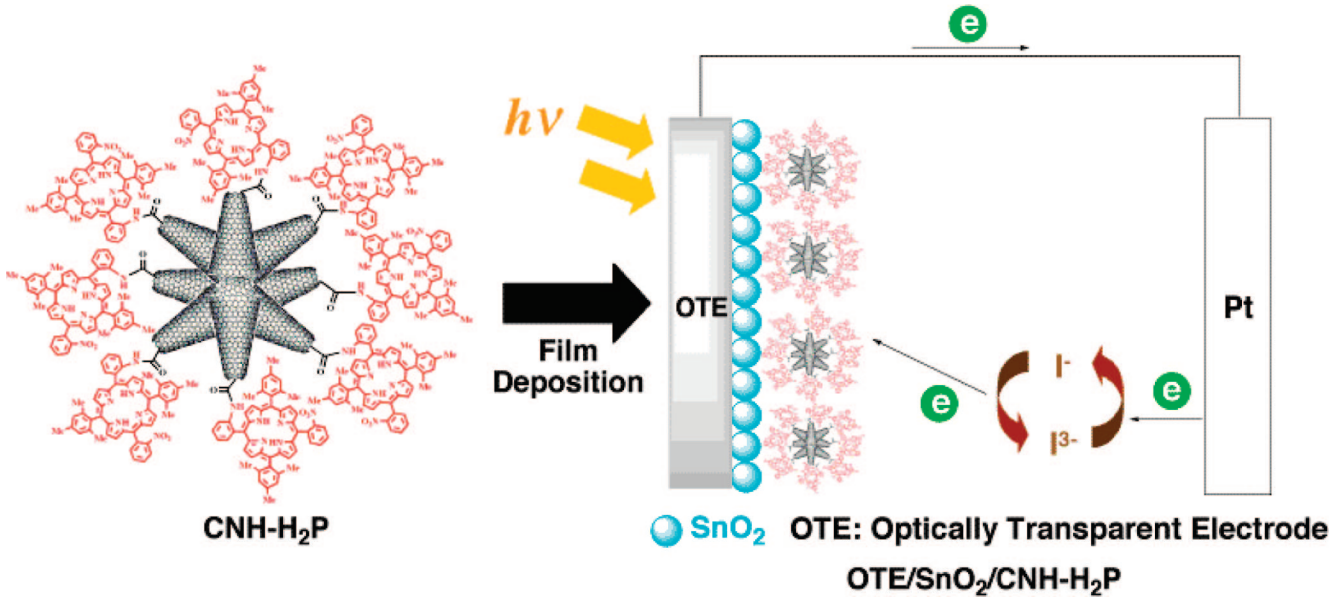

photosensitive electrode in a photoelectrochemical cell, as shown in Scheme 1.

Experimental Section

General Information. The UV−vis spectra were recorded on a Perkin-Elmer (Lamda 750) UV−vis−NIR spectrophotometer. Scanning electron microscopy images were recorded with a Hitachi S-4100 scanning electron microscope. Emission spectra were recorded on a Perkin-Elmer (LS-55) spectrofluorophotometer equipped with a photomultiplier tube having high sensitivity in the 400−800 nm region.

Materials. All solvents and chemicals were of reagent grade quality, obtained commercially and used without further purification unless otherwise noted. The synthesis and chemical characterization of porphyrin utilized in this study and the covalent functionalized CNH−H_2P hybrid material have been previously reported.[29] Preparation of OTE coated with the nanostructured SnO_2 film is as follows:[33] a dilute (∼5%) SnO_2 colloidal aqueous solution (Alpha Chemicals, particle size: ∼15 nm) was repeatedly sprayed onto the OTE electrode (ITO/ATO film from Geomatec Co., Ltd., Japan, sheet resistance: ∼8 Ω/square), followed by annealing at 673 K for ∼0.5 h. The thickness of SnO_2 on an OTE film was measured as ∼10 μm by Dektak 3030 (Veeco Instruments). The OTE coated with the nanostructured SnO_2 film is referred to as OTE/SnO_2.

Electrophoretic Deposition of CNH−H_2P Films. Pristine CNHs (1.20 mg) in THF (10 mL) and functionalized CNH−H_2P (1.40 mg) in THF (10 mL), respectively, were transferred to a 1 cm cuvette in which two electrodes (viz., OTE/SnO_2 and OTE) were kept at a distance of 6 mm with a Teflon spacer. A dc electric field (∼100 V cm^{-1}) was applied for 2 min between these two electrodes using a PowerPac HV (Biorad).[34] The deposition of the film was visible as the solution becomes colorless with simultaneous black coloration of the OTE/SnO_2 electrode. The OTE/SnO_2 electrodes coated with pristine CNHs and porphyrins are referred to as OTE/SnO_2/CNH and OTE/SnO_2/H_2P, respectively, and the one which is coated with molecular assemblies of covalent functionalized CNH−H_2P is referred to as OTE/SnO_2/CNH−H_2P. In OTE/SnO_2/H_2P and OTE/SnO_2/CNH films, 15% H_2P moieties and 85% CNH (weight ratio) toward total weight of CNH−H_2P was deposited onto OTE/SnO_2 since the detail structural information has been reported previously.[29] With regard to the preparation of the OTE/SnO_2/H_2P film, the H_2P solution was directly sprayed onto the OTE/SnO_2.

Photoelectrochemical Measurements. Photoelectrochemical measurements were carried out in a standard two-compartment cell consisting of a working electrode, a Pt wire gauze counter electrode. In the measurement of a three-compartment cell using potentiostat, we additionally employed a saturated calomel reference electrode (SCE).[14] This configuration allowed us to carry out photocurrent measurements under electrochemical bias.[34] The detailed measurement information of two- and three-electrode systems have been reported previously.[34] IviumStat (potentiostat) was used for recording $I-V$ characteristics and photocurrent generation density. The electrolyte is 0.5 M LiI and 0.01 M I_2 in acetonitrile. A collimated light beam from a 300 W xenon lamp with a AM 1.5 filter was used for excitation of a porphyrin assembly film deposited on an OTE film. In the case of measurement of IPCE spectra, a monochromator (SM-25, Bunkoh-Keiki Co., Ltd.) was introduced into the path of the excitation beam for the selected wavelength.

Fluorescence Lifetime Measurements. The time-resolved fluorescence spectra were measured by single photon counting method using a streakscope (Hamamatsu Photonics, C5680) as a detector and the laser light (Hamamatsu Photonics M10306, laser diode head, 408 nm) as an excitation source. Lifetimes were evaluated with software supplied with the instrumentation.

Nanosecond Transient Absorption Spectroscopy. Nanosecond transient absorption measurements were carried out using THG (532 nm) of a Nd:YAG laser (Spectra-Physics, Quanta-Ray GCR-250−10, 6 ns fwhm) as an excitation source. For transient absorption spectra and the time-profiles, monitoring light from a pulsed Xe Flash lamp (Hamamatsu Photonics C4479) was detected with CCD detector equipped with an image intensifier, ICCD-1024G (Princeton Instruments). The time profile was evaluated with software supplied with the instrumentation (WinSpec software).

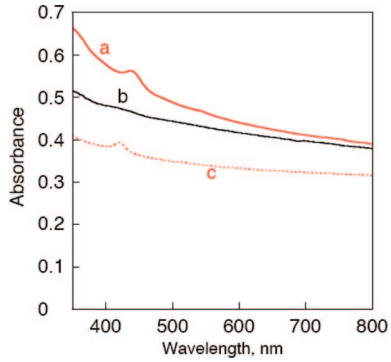

Figure 1. Steady-state absorption spectra of the (a) OTE/SnO_2/CNH−H_2P film, (b) OTE/SnO_2/CNH film, and (c) CNH−H_2P solution in THF (about 0.03 mg/mL).

Results and Discussion

Electrophoretic Deposition. Electrophoretic deposition was applied to fabricate films of CNH onto OTE and nanostructured SnO_2 films cast onto OTE (OTE/SnO_2).[17,34] A suspension of the CNH (∼2 mL) in THF was transferred to a 1 cm cuvette. Two OTE cut from conducting glass were inserted, and a dc electric field (∼100 V/cm) was applied. The CNH from the suspension were driven to the positive electrode surface, and a robust thin film (abbreviated as OTE/SnO_2/CNH) was deposited within 2 min. An analogous process was adopted to deposit the functionalized CNH−H_2P nanoassemblies onto OTE/SnO_2 (abbreviated as OTE/SnO_2/CNH−H_2P). The steady-state electron absorption spectra of the OTE/SnO_2/CNH−H_2P and OTE/SnO_2/CNH electrodes as compared with the absorption spectrum of CNH−H_2P in THF are shown in Figure 1.

The OTE/SnO_2/CNH−H_2P film absorbs incident light effectively in the visible region, and the absorption band extends into the near-infrared region (Figure 1a). At the UV−vis spectra of CNH−H_2P in solution (Figure 1c), the characteristic Soret band due to the porphyrin unit is identified (the Q bands are broadened and flattened in the baseline of the spectrum) while the presence of CNHs is proved by the continuous absorbance from the UV−vis to the NIR regions. Moreover, the same Soret band in the OTE/SnO_2/CNH−H_2P film is identified (Figure 1a), broadened and red-shifted by approximately 20 nm, as compared with the corresponding bands of the CNH−H_2P in THF solution. The broader absorption of the electrodes is likely to arise from the clustering effects of porphyrin moieties or electronic interaction between CNH and H_2P, the details of which can be found elsewhere.[34] In contrast, the absorption spectra of OTE/SnO_2/CNH (Figure 1b) shows only the continuous absorbance from the UV−vis to the NIR region due to the presence of carbon nanohorns thus proving the assignment of continuous absorbance in the OTE/SnO_2/CNH−H_2P film (Figure 1a) to CNH.

Surface Characterization of CNH−H_2P Films. Scanning electron microscopy (SEM) for the morphological characterization of the above electrodes was performed. The microscope images of the OTE/SnO_2/CNH−H_2P film and of OTE/SnO_2/CNH are shown in Figure 2, respectively.

A close inspection of these images reveals a tightly packed assembly of the pristine and modified carbon nanohorns on film. Based on these images, the average aggregate sizes of CNH−H_2P composites and pristine CNHs are ca. 60−100 nm (Figure 1A). Since the aggregate diameter of CNHs is reported as 80−100 nm,[20] we can conclude that the aggregate structures were effectively transferred onto the OTE/SnO_2 film. Additionally, the average sizes of CNH−H_2P composites are very similar to those of pristine CNHs (vide supra). This suggests that further aggregations via porphyrin moieties do not occur in the CNH−H_2P composites. The micrographs confirm the presence of the materials in the surface of the electrodes and the ability of electrophoresis to assemble CNHs and covalent functionalized CNH−H_2P onto the electrode surface.

Photocurrent Generation Properties of CNH−H_2P Films. Photoelectrochemical measurements were performed in acetonitrile containing 0.5 M LiI and 0.01 M I_2 as the redox electrolyte with OTE/SnO_2/CNH−H_2P and OTE/SnO_2/CNH as the working electrode and Pt wire as the counter electrode. The photoelectrochemical performance of the OTE/SnO_2/CNH−H_2P electrode was examined by employing a standard two-compartment cell with a Pt wire gauge counter electrode.[6] In Figure 3 are shown the photocurrent responses of the OTE/SnO_2/CNH−H_2P and OTE/SnO_2/CNH electrodes. The photocurrent responses are prompt, steady, and reproducible during repeated on/off cycles of the visible light illumination. The short circuit photocurrent (I_{sc}) of the OTE/SnO_2/CNH−H_2P electrode is 0.25 mA cm^{-2} (Figure 3A) under white light illumination (AM 1.5 condition; input power = 80 mW cm^{-2}), and this value is nearly two times greater than that (0.12 mA cm^{-2}) obtained with the OTE/SnO_2/CNH electrode (Figure 3B), while the I_{sc} value of OTE/TiO_2/CNH shows nearly zero current (Figure 3C).[35]

Furthermore, an evaluation of the photocurrent action spectrum of the OTE/SnO_2/CNH−H_2P electrode with those of the single-component electrode systems, such as the OTE/SnO_2/CNH and the OTE/SnO_2/H_2P electrodes, was performed, by examining the wavelength dependence of the incident photon to current conversion efficiency (IPCE). The IPCE values are calculated by normalizing the photocurrent densities for incident light energy and intensity and by use of the following expression:[7]

$$\mathrm{IPCE}(\%) = 100 \times 1240 \times i/(W_{in} \times \lambda)$$

where i is the photocurrent density (A cm^{-2}), W_{in} is the incident light intensity (W cm^{-2}), and λ is the excitation wavelength (nm). As shown in Figure 4, the photocurrent action spectrum of the OTE/SnO_2/CNH−H_2P electrode shows a maximum IPCE value of 2.7% at 440 nm (Figure 4a). Following the same experimental conditions, the observed IPCE values for single-component systems, namely OTE/SnO_2/CNH and OTE/SnO_2/H_2P electrodes, are relatively much smaller, 1.4% and 0.3% at 440 nm, respectively, as indicated in the spectra b and c in Figure 4, respectively.

Finally, it was necessary to investigate the photocurrent action spectra of the OTE/SnO_2/CNH and OTE/SnO_2/H_2P electrodes to see whether the enhancement seen in the photocurrent was an additive effect or not. Spectrum of Figure 4d shows the additive spectra obtained from the spectra of Figures 4b and 4c. If the enhancement in the photocurrent generation was simply an additive result, the response of the composite electrode would have been similar to that of spectrum in Figure 4d with a maximum IPCE around 1.8% at 440 nm. However, an IPCE of 2.7% with the OTE/SnO_2/CNH−H_2P electrode at 440 nm was obtained. The experimental observation of the photocurrent enhancement generation is a valuable clue of the interaction between the excited porphyrin which is covalently bonded to CNHs, ordering the overall photocurrent generation.

The charge separation in the OTE/SnO_2/CNH−H_2P electrode can be further modulated by the application of an electrochemical bias potential (a standard three-compartment cell as a working electrode along with Pt wire gauze counter electrode and saturated calomel reference electrode). Figure 5A shows

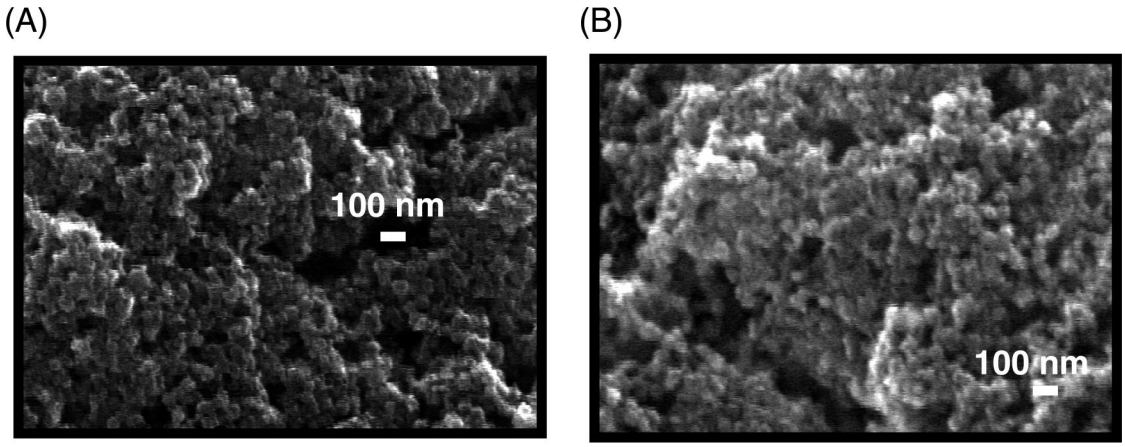

Figure 2. Scanning electron microscopy images of (A) CNH−H_2P on the OTE/SnO_2 film and (B) CNHs on the OTE/SnO_2 film, prepared by electrophoretic deposition method.

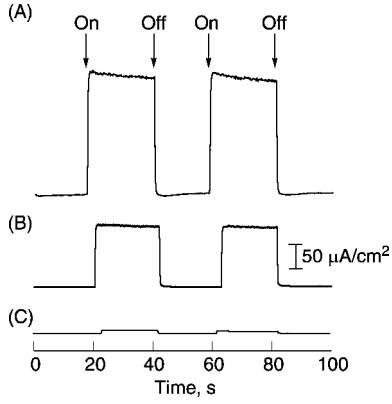

Figure 3. Photocurrent generation responses of (A) OTE/SnO_2/CNH−H_2P, (B) OTE/SnO_2/CNH, and (C) OTE/TiO_2/CNH under white light illumination using an AM 1.5 filter. Input power: 80 mW cm^{-2}.

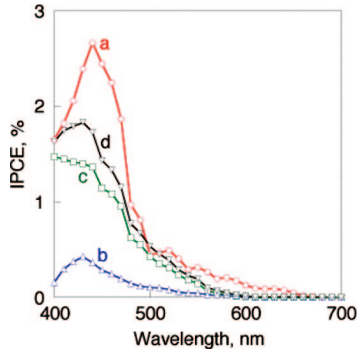

Figure 4. Photocurrent action spectra of (a) OTE/SnO_2/CNH−H_2P, (b) OTE/SnO_2/H_2P, (c) OTE/SnO_2/CNH, and (d) the sum of spectra b (OTE/SnO_2/H_2P) and c (OTE/SnO_2/CNH) under a standard two-compartment cell. Electrolyte: 0.5 M LiI and I_2 0.01 M in acetonitrile; working electrode: OTE/SnO_2/CNH−H_2P or OTE/SnO_2/H_2P film; counter electrode: Pt wire.

$I-V$ characteristics of the OTE/SnO_2/CNH−H_2P under visible light illumination (AM 1.5). The photocurrent increases as the applied potential is scanned toward more positive potentials. Increased charge separation and the facile transport of charge carriers under a positive bias potential are responsible for enhanced photocurrent generation. At potentials greater than +0.3 V vs SCE, the direct electrochemical oxidation of iodide interferes with the photocurrent measurement. The net photocurrent generation density of OTE/SnO_2/CNH−H_2P at +0.2 V vs SCE (~0.55 mA/cm^2) was much larger than the case at 0 V vs SCE (~0.20 mA/cm^2).[34] Thus, by using a three-compartment cell, we can control photocurrent generation density of the OTE/SnO_2/CNH−H_2P electrode.

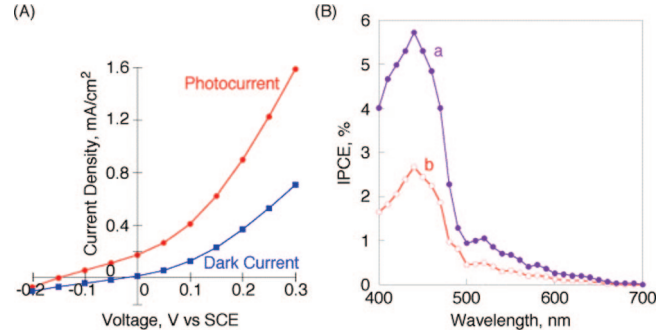

Figure 5. (A) $I-V$ characteristics of the OTE/SnO_2/CNH−H_2P electrode under white light illumination (AM 1.5 conditions). Electrolyte: LiI 0.5 M, I_2 0.01 M in acetonitrile; input power = 80 mW cm^{-2}. (B) Photocurrent action spectra of the OTE/SnO_2/CNH−H_2P electrode (a) at an applied bias potential of 0.2 V vs SCE and (b) without applied bias potential. Electrolyte: LiI 0.5 M, I_2 0.01 M in acetonitrile.

By controlling the potential of OTE/SnO_2 with an electrochemical bias, we can improve the charge separation and attain higher IPCE values.[6b] The photocurrent action spectra of OTE/SnO_2/CNH−H_2P under an applied bias potential of 0.2 V vs SCE were recorded using a standard three-compartment cell. The IPCE values of OTE/SnO_2/CNH−H_2P under an applied bias potential of 0.2 V vs SCE (spectrum a in Figure 5) are much larger than those under no applied voltage condition (spectrum b) in the whole visible region. The maximum IPCE values of OTE/SnO_2/CNH−H_2P at 0.2 V vs SCE attains 5.8%, which is more than two times larger than that at 0 V vs SCE (2.7%). This trend is in good agreement with $I-V$ characteristics (Figure 5A). The maximum IPCE value (5.8%) is slightly low as compared to our previous systems composed of carbon nanotube composites[14d] while with a similar value when compared with a covalently linked porphyrin to the carbon nanotube[14e] (because of covalent linkage between CNH and H_2P).[36] Although the limited and isolated porphyrin monolayers covalently attached onto a CNH surface may hamper efficient carrier transport after photoinduced electron transfer (PET), we can efficiently evaluate the PET process effect between the carbon nanotube and porphyrin moiety on the light energy conversion property because of the covalent attachment in this system. These results clearly ensure that the PET process in the CNH−H_2P system plays an important role in the light energy conversion (vide infra). On the basis of these photoelectro-

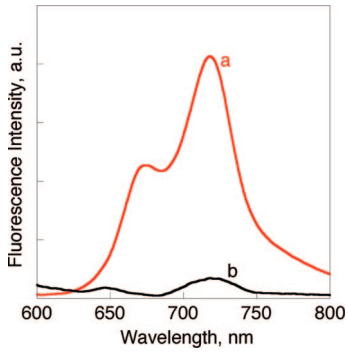

Figure 6. Steady-state fluorescence spectra of (a) OTE/SnO_2/H_2P film and (b) OTE/SnO_2/CNH−H_2P film (λ_{exc} = 520 nm).

chemical experiments, we can conclude that organization of molecular assemblies achieved with CNH−H_2P is a key factor in attaining improved light energy conversion properties.

Electronic Interactions between the Excited H_2P and CNHs in the OTE/SnO_2/CNH−H_2P Film. In a previous investigation of the interactions between the excited H_2P and CNHs in the CNH−H_2P nanoensemble, there was strong evidence for electron transfer. The photoexcitation of the porphyrin moiety that resulted in the reduction of CNHs with a simultaneous oxidation of the H_2P unit revealed the charge-separated state of $CNH^{\bullet-}$−$H_2P^{\bullet+}$ which was confirmed with the aid of an electron mediator, such as hexyl-viologen dication (HV^{2+}) in polar solvents. Furthermore, the charge-separated states of $CNH^{\bullet-}$−$H_2P^{\bullet+}$ were identified with the aid of transient absorption spectroscopy.[29]

Moving a step forward and for the purposes of the current study, a similar investigation for the electron communication has been carried out in the OTE/SnO_2/CNH−H_2P film. In detail, a comparison of the steady-state fluorescence spectra and fluorescence lifetimes of OTE/SnO_2/CNH−H_2P and OTE/SnO_2/H_2P films have been performed. Figure 6 compares the steady-state fluorescence spectra of the OTE/SnO_2/H_2P film (spectrum a) and OTE/SnO_2/CNH−H_2P film (spectrum b) with matched absorbance at 420 nm. The excitation wavelength is 520 nm. The H_2P assembly film shows a twin peak with maximum at 670 and 720 nm. The fluorescence intensity of CNH−H_2P film exhibits a notably lower emission yield, thus confirming the quenched excited state. The maximum peak of the OTE/SnO_2/CNH−H_2P film at shorter wavelength (∼650 nm) is approximately in agreement with that in solution[29] although blue-shifted as compared to that of OTE/SnO_2/H_2P (∼670 nm).

For the acquisition of further information regarding the kinetics and mechanistic details of electron-transfer process, it was necessary to measure the fluorescence lifetime of the OTE/SnO_2/CNH−H_2P film and compare it with that of OTE/SnO_2/H_2P (Figure 7). The emission decay of the H_2P film deviates from the monoexponential decay behavior and can be fitted to the biexponential decay kinetics. The lifetime of the OTE/SnO_2/H_2P film was 710 ps, which is shorter than that in solution because of aggregation of H_2P moieties on film. The excited H_2P in the OTE/SnO_2/CNH−H_2P electrode revealed the presence of two lifetime components, both which deactivated faster than that in the OTE/SnO_2/H_2P electrode. The emission decay was analyzed by using the biexponential kinetic fit, and the lifetimes are summarized in Table 1. A 75% level of decay occurred via a very fast deactivation pathway, near 90 ps. This fast decay component could be ascribed to the electron-transfer pathway of excited-state deactivation. On the basis of these results, the forward electron transfer rate constant in CNH−H_2P onto OTE/SnO_2 film, k_{ET} is determined as 9.7×10^9 s^{-1}.[37]

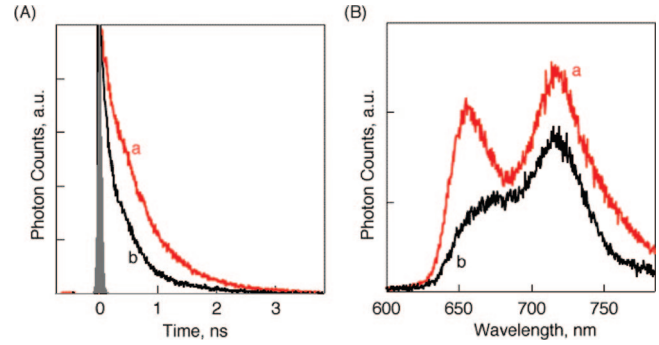

Figure 7. (A) Fluorescence decay profiles of (a) OTE/SnO_2/H_2P film and (b) OTE/SnO_2/CNH−H_2P films (λ_{exc} = 408 nm) and (B) time-resolved fluorescence spectra (∼50 ps) of (a) OTE/SnO_2/H_2P film and (b) OTE/SnO_2/CNH−H_2P film (λ_{exc} = 408 nm).

TABLE 1: Summary of Fluorescence Lifetime of the OTE/SnO_2/CNH−H_2P Film

sample	lifetime, τ_f	k_{ET},[a] s^{-1}
OTE/SnO_2/CNH−H_2P	90 ps (75%), 500 ps (25%)	9.7×10^9
OTE/SnO_2/H_2P	710 ps (100%)	–
H_2P in toluene	4900 ps (100%)	–

[a] Calculated by $k_{ET} = (1/\tau_f)_{sample} - (1/\tau_f)_{ref}$; the value of $(\tau_f)_{ref}$ was 710 ps for OTE/SnO_2/H_2P.

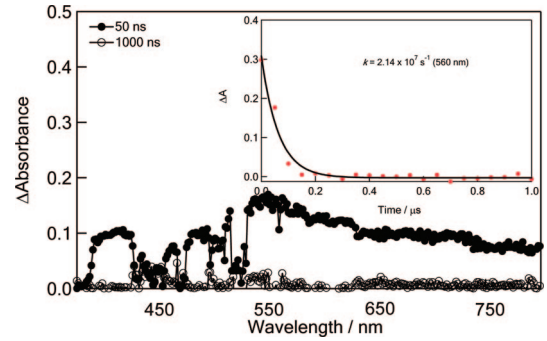

Figure 8. Nanosecond transient absorption spectra of the OTE/SnO_2/CNH−H_2P film observed by 532 nm (ca. 4 mJ/pulse) laser irradiation. Inset: Absorption-time profile.

Finally, additional support derives from transient absorption measurements, following 532 nm laser irradiation of the OTE/SnO_2/CNH−H_2P film. By photoexciting the Q-band of H_2P, i.e. at 532 nm, with short laser pulses, the transient photoproducts are identified and their decay rates are resolved.The transient absorption bands in the visible region were observed, as shown in Figure 8. The absorption band observed in the visible region near 550 nm corresponds to the one-electron oxidized product, namely $H_2P^{\bullet+}$.[29,38] The charge recombination rate constant of CNH−H_2P on OTE/SnO_2 is determined to be 2.14×10^7 s^{-1}, which corresponds to 47 ns for $H_2P^{\bullet+}$. Although the transient spectrum in the near-infrared region is not observed in this setup, the spectral trend is in good agreement with our previous spectrum in solution.[29] Additionally, on the basis of this light energy conversion property, fluorescence lifetime, and transient absorption measurements, we can conclude that photoinduced charge-separated state of $CNH^{\bullet-}$−$H_2P^{\bullet+}$ contributes to the enhancement of the light energy conversion property in the photoelectrochemical solar cell.

On the basis of these results, we conclude that the photoinduced electron transfer occurs from the singlet excited state of H_2P ($^1H_2P^*/H_2P^{\bullet+} = -0.7$ V vs NHE)[29,34] to CNH during the irradiation of the CNH−H_2P composite assembly. As shown

earlier, the conduction band of semiconducting CNH is in the range of −0.5 and 0 V vs NHE.[35] Such energetics of the CNH favors charge injection from the excited porphyrin into CNH. The reduced CNH injects electrons into the SnO_2 nanocrystallites to generate photocurrent. The oxidized porphyrin ($H_2P/H_2P^{+\bullet}$ = 1.2 V vs NHE)[29, 33] undergoes electron-transfer reduction with the iodide (I_3^-/I^- = 0.5 V vs NHE) couple present in the electrolyte.[29,33] By using the regenerative redox cycle we are able to maintain a steady flow of photocurrent.

Conclusion

Photoelectrochemical electrodes of porphyrin-functionalized CNH−H_2P, carbon nanohorns, have been constructed for the first time. The film of the CNH−H_2P onto the nanostructured SnO_2 electrode exhibited an incident photon-to-photocurrent efficiency (IPCE) of 5.8% in a three-compartment electrochemical cell. The measured IPCE has been found greater than the one observed for the sum of the single components, namely CNHs and H_2P, onto the nanostructured SnO_2 electrode. Fluorescence lifetime measurements revealed that electron transfer from the singlet excited state of the porphyrin to the nanohorns takes place. In addition, direct electron injection from the reduced nanohorns to the conduction band of the SnO_2 electrode occurs. These processes are responsible for the photocurrent generation. The results obtained demonstrate the potentiality and applied utility of carbon nanohorns in directing efficient charge transport in photoelectrochemical devices.

Acknowledgment. This work, made under the European Heads of Research Councils and European Science Foundation EURYI (European Young Investigator) Awards scheme, was partially supported by funds from the Participating Organizations of EURYI and the EC Sixth Framework Program. Partial financial support from the EU FP7, Capacities Program, NANOHOST project (GA 201729) is also acknowledged. This work was also supported by Grant-in-Aids for Scientific Research (No. 19710119 to T.H.) and special coordination funds for promoting science and technology from the Ministry of Education, Culture, Sports, Science and Technology, Japan.

References and Notes

(1) (a) Dresselhaus, M. S.; Dresselhaus, G.; Eklund, P. C. *Science of Fullerenes and Carbon Nanotubes*; Academic Press: San Diego, 1996. (b) Kadish, K. D.; Ruoff, R. S., Eds. *Fullerenes*; Wiley: New York, 2000. (c) Reich, S.; Thomsen, C.; Maultzsch, J. *Carbon Nanotubes*; Wiley-VCH: Weinheim, 2004. (d) Rotkin, S. V.; Subramoney, S., Eds. *Applied Physics of Carbon Nanotubes*; Springer: Berlin, 2005. (e) Brabec, C.; Dyakonov, V.; Parisi, J.; Sariciftci, N. S., Eds. *Organic Photovoltaics*; Springer: Berlin, 2003.

(2) (a) Guldi, D. M. *J. Phys. Chem. B* **2005**, *109*, 11432. (b) Katz, E.; Willner, I. *ChemPhysChem* **2004**, *5*, 1084. (c) Kamat, P. V. *J. Phys. Chem. C* **2007**, *111*, 2834.

(3) (a) Imahori, H.; Hagiwara, K.; Akiyama, T.; Aoki, M.; Taniguchi, S.; Okada, T.; Shirakawa, M.; Sakata, Y. *Chem. Phys. Lett.* **1996**, *263*, 545. (b) Imahori, H.; Yamada, H.; Guldi, D. M.; Endo, Y.; Shimomura, A.; Kundu, S.; Yamada, K.; Okada, T.; Sakata, Y.; Fukuzumi, S. *Angew. Chem., Int. Ed.* **2002**, *41*, 2344. (c) Fukuzumi, S.; Ohkubo, K.; Imahori, H.; Guldi, D. M. *Chem. Eur. J.* **2003**, *9*, 1585.

(4) (a) Kamat, P. V.; Barazzouk, S.; Thomas, K. G.; Hotchandani, S. *J. Phys. Chem. B* **2000**, *104*, 4014. (b) Kamat, P. V.; Barazzouk, S.; Hotchandani, S.; Thomas, K. G. *Chem. Eur. J.* **2000**, *6*, 3914.

(5) Imahori, H. *J. Mater. Chem.* **2007**, *17*, 31.

(6) (a) Imahori, H.; Hasobe, T.; Yamada, H.; Kamat, P. V.; Barazzouk, S.; Fujitsuka, M.; Ito, O.; Fukuzumi, S. *Chem. Lett.* **2001**, 784. (b) Hasobe, T.; Imahori, H.; Fukuzumi, S.; Kamat, P. V. *J. Phys. Chem. B* **2003**, *107*, 12105.

(7) (a) Hasobe, T.; Kashiwagi, Y.; Absalom, M. A.; Sly, J.; Hosomizu, K.; Crossley, M. J.; Imahori, H.; Kamat, P. V.; Fukuzumi, S. *Adv. Mater.* **2004**, *16*, 975. (b) Hasobe, T.; Kamat, P. V.; Absalom, M. A.; Kashiwagi, Y.; Sly, J.; Crossley, M. J.; Hosomizu, K.; Imahori, H.; Fukuzumi, S. *J. Phys. Chem. B* **2004**, *118*, 12865.

(8) Hasobe, T.; Kamat, P. V.; Troiani, V.; Solladie, N.; Ahn, T. K.; Kim, S. K.; Kim, D.; Kongkanand, A.; Kuwabata, S.; Fukuzumi, S. *J. Phys. Chem. B* **2005**, *109*, 19.

(9) (a) Hasobe, T.; Imahori, H.; Kamat, P. V.; Fukuzumi, S. *J. Am. Chem. Soc.* **2003**, *125*, 14962. (b) Hasobe, T.; Hattori, S.; Kamat, P. V.; Urano, Y.; Umezawa, N.; Nagano, T.; Fukuzumi, S. *Chem. Phys.* **2005**, *319*, 243. (c) Hasobe, T.; Imahori, H.; Kamat, P. V.; Ahn, T. K.; Kim, S. K.; Kim, D.; Fujimoto, A.; Hirakawa, T.; Fukuzumi, S. *J. Am. Chem. Soc.* **2005**, *127*, 1216. (d) Imahori, H.; Fujimoto, A.; Kang, S.; Hotta, H.; Yoshida, K.; Umeyama, T.; Matano, Y.; Isoda, S.; Isosomppi, M.; Tkachenko, N. V.; Lemmetyinen, H. *Chem. Eur. J.* **2005**, *11*, 7265. (e) Imahori, H.; Mitamura, K.; Shibano, Y.; Umeyama, T.; Matano, Y.; Yoshida, K.; Isoda, S.; Araki, Y.; Ito, O. *J. Phys. Chem. B* **2006**, *110*, 11399.

(10) Kang, S.; Umeyama, T.; Ueda, M.; Matano, Y.; Hotta, H.; Yoshida, K.; Isoda, S.; Shiro, M.; Imahori, H. *Adv. Mater.* **2006**, *18*, 2549.

(11) (a) Romero, D. B.; Carrard, M.; Heer, W. D.; Zuppiroli, L. *Adv. Mater.* **1996**, *8*, 899. (b) Ago, H.; Petritsch, K.; Shaffer, M. S. P.; Windle, A. H.; Friend, R. H. *Adv. Mater.* **1999**, *11*, 1281. (c) Star, A.; Stoddart, J. F.; Steuerman, D.; Diehl, M.; Boukai, A.; Wong, E. W.; Yang, X.; Chung, S.-W.; Choi, H.; Heath, J. R. *Angew. Chem., Int. Ed.* **2001**, *40*, 1721.

(12) (a) Kymakis, E.; Amaratunga, G. A. J. *Appl. Phys. Lett.* **2002**, *80*, 112. (b) Bhattacharyya, S.; Kymakis, E.; Amaratunga, G. A. J. *Chem. Mater.* **2004**, *16*, 4819. (c) Landi, B. J.; Raffaelle, R. P.; Castro, S. L.; Bailey, S. G. *Prog. Photovolt.: Res. Appl.* **2005**, *13*, 165. (d) Pradhan, B.; Batabyal, S. K.; Pal, A. J. *Appl. Phys. Lett.* **2006**, *88*, 093106.

(13) (a) Wu, W.; Li, J.; Liu, L.; Yanga, L.; Guo, Z.-X.; Dai, L.; Zhu, D. *Chem. Phys. Lett.* **2002**, *364*, 196. (b) Jang, S.-R.; Vittal, R.; Kim, K.-J. *Langmuir* **2004**, *20*, 9807. (c) Rahman, G. M. A.; Guldi, D. M.; Cagnoli, R.; Mucci, A.; Schenetti, L.; Vaccari, L.; Prato, M. *J. Am. Chem. Soc.* **2005**, *127*, 10051. (d) Sheeney-Haj-Ichia, L.; Basnar, B.; Willner, I. *Angew. Chem., Int. Ed.* **2005**, *44*, 78. (e) Sgobba, V.; Rahman, G. M. A.; Guldi, D. M.; Jux, N.; Campidelli, S.; Prato, M. *Adv. Mater.* **2006**, *18*, 2264.

(14) (a) Barazzouk, S.; Hotchandani, S.; Vinodgopal, K.; Kamat, P. V. *J. Phys. Chem. B* **2004**, *108*, 17015. (b) Robel, I.; Bunker, B. A.; Kamat, P. V. *Adv. Mater.* **2005**, *17*, 2458. (c) Hasobe, T.; Fukuzumi, S.; Kamat, P. V. *J. Am. Chem. Soc.* **2005**, *127*, 11884. (d) Hasobe, T.; Fukuzumi, S.; Kamat, P. V. *J. Phys. Chem. B* **2006**, *110*, 25477. (e) Umeyama, T.; Fujita, M.; Tezuka, N.; Kadota, N.; Matano, Y.; Yoshida, K.; Isoda, S.; Imahori, H. *J. Phys. Chem. C* **2007**, *111*, 11484.

(15) Ma, Y. Z.; Valkunas, L.; Bachilo, S. M.; Fleming, G. R. *J. Phys. Chem. B* **2005**, *109*, 15671.

(16) Strano, M. S.; Dyke, C. A.; Usrey, M. L.; Barone, P. W.; Allen, M. J.; Shan, H.; Kittrell, C.; Hauge, R. H.; Tour, J. M.; Smalley, R. E. *Science* **2003**, *301*, 1519.

(17) Barazzouk, S.; Hotchandani, S.; Vinodgopal, K.; Kamat, P. V. *J. Phys. Chem. B* **2004**, *108*, 17015.

(18) Kamat, P. V.; Thomas, K. G.; Barazzouk, S.; Girishkumar, G.; Vinodgopal, K.; Meisel, D. *J. Am. Chem. Soc.* **2004**, *126*, 10757.

(19) (a) Hasobe, T.; Fukuzumi, S.; Kamat, P. V. *J. Phys. Chem. B* **2006**, *110*, 25477. (b) Saito, K.; Ohtani, M.; Fukuzumi, S. *J. Am. Chem. Soc.* **2006**, *128*, 14216. (c) Hasobe, T.; Fukuzumi, S.; Kamat, P. V. *Angew. Chem., Int. Ed.* **2006**, *45*, 755. (d) Saito, K.; Ohtani, M.; Fukuzumi, S. *Chem. Commun.* **2007**, 55. (e) Fukuzumi, S.; Kojima, T. *J. Mater. Chem.* **2008**, *18*, 1427.

(20) Iijima, S.; Yudasaka, M.; Yamada, R.; Bandow, S.; Suenaga, K.; Kokai, F.; Takahashi, K. *Chem. Phys. Lett.* **1999**, *309*, 165.

(21) (a) Petsalakis, I. D.; Pagona, G.; Theodorakopoulos, G.; Tagmatarchis, N.; Yudasaka, M.; Iijima, S. *Chem. Phys. Lett.* **2006**, *429*, 194. (b) Petsalakis, I. D.; Pagona, G.; Tagmatarchis, N.; Theodorokapoulos, G. *Chem. Phys. Lett.* **2007**, *448*, 115.

(22) (a) Tagmatarchis, N.; Maigné, A.; Yudasaka, M.; Iijima, S. *Small* **2006**, *2*, 490. (b) Pagona, G.; Tagmatarchis, N.; Fan, J.; Yudasaka, M.; Iijima, S. *Chem. Mater.* **2006**, *18*, 3918. (c) Mountrichas, G.; Pispas, S.; Tagmatarchis, N. *Chem. Eur. J.* **2007**, *13*, 7595. (d) Pagona, G.; Karousis, N.; Tagmatarchis, N. *Carbon* **2008**, *46*, 604.

(23) Cioffi, C.; Campidelli, S.; Brunetti, F. G.; Meneghetti, M.; Prato, M. *Chem. Commun.* **2006**, 2129.

(24) Isobe, H.; Tanaka, T.; Maeda, R.; Noiri, E.; Solin, N.; Yudasaka, M.; Iijima, S.; Nakamura, E. *Angew. Chem., Int. Ed.* **2006**, *45*, 6676.

(25) Zhang, M.; Yudasaka, M.; Ajima, K.; Miyawaki, J.; Iijima, S. *ACS Nano* **2007**, *1*, 265.

(26) Sandanayaka, A. S. D.; Pagona, G.; Tagmatarchis, N.; Yudasaka, M.; Iijima, S.; Araki, Y.; Ito, O. *J. Mater. Chem.* **2007**, *17*, 2540.

(27) Pagona, G.; Sandanayaka, A. S. D.; Araki, Y.; Fan, J.; Tagmatarchis, N.; Yudasaka, M.; Iijima, S.; Ito, O. *J. Phys. Chem. B* **2006**, *110*, 20729.

(28) Pagona, G.; Fan, J.; Maignè, A.; Yudasaka, M.; Iijima, S.; Tagmatarchis, N. *Diamond Relat. Mater.* **2007**, *16*, 1150.

(29) Pagona, G.; Sandanayaka, A. S. D.; Araki, Y.; Fan, J.; Tagmatarchis, N.; Charalambidis, G.; Coutsolelos, A. G.; Boitrel, B.; Yudasaka, M.; Iijima, S.; Ito, O. *Adv. Funct. Mater.* **2007**, *17*, 1705.

(30) Cioffi, C.; Campidelli, S.; Sooambar, C.; Marcaccio, M.; Marcolongo, G.; Meneghetti, M.; Paolucci, D.; Paolucci, F.; Ehli, C.; Rahman, G. M. A.; Sgobba, V.; Guldi, D. M.; Prato, M. *J. Am. Chem. Soc.* **2007**, *129*, 3938.

(31) Pagona, G.; Rotas, G.; Petsalakis, I. D.; Theodorakopoulos, G.; Maigné, A.; Fan, J.; Yudasaka, M.; Iijima, S.; Tagmatarchis, N. *J. Nanosci. Nanotechnol.* **2007**, *7*, 3468.

(32) Pagona, G.; Sandanayaka, A. S. D.; Maigń; e, A.; Fan, J.; Papavassiliou, G. C.; Petsalakis, I. D.; Steele, B. R.; Tagmatarchis, N.; Yudasaka, M.; Iijima, S.; Ito, O. *Chem. Eur. J.* **2007**, *13*, 7600.

(33) Bedja, I.; Hotchandani, S.; Kamat, P. V. *J. Phys. Chem.* **1994**, *98*, 4133.

(34) Hasobe, T.; Imahori, H.; Fukuzumi, S.; Kamat, P. V. *J. Phys. Chem. B* **2003**, *107*, 12105.

(35) The I_{sc} value of OTE/TiO_2/CNH is nearly zero current (Figure 3C). This indicates that the electron transfer from excited CNHs to SnO_2 nanocrystallites (conduction band: ∼−0 vs NHE) is exergonic, while that from excited CNHs to TiO_2 nanocrystallites (conduction band: ∼−0.5 vs NHE) is endergonic. The conduction band of the CNHs lies between 0 and−0.5 V vs NHE. See the following reference paper: Hasobe, T.; Fukuzumi, S.; Kamat, P. V. *Angew. Chem., Int. Ed.* **2006**, *45*, 755.

(36) We performed IPCE measurement of the composite film composed of CNH reference and H_2P reference under no applied bias condition. IPCE value of OTE/SnO_2/CNH−H_2P (∼2.7%) is slightly higher than that in the reference system (∼2.4%) at 440 nm.

(37) It should be noted that this value is an upper estimate, and other components may also contribute to the electron-transfer process.

(38) (a) Rodriguez, J.; Kirmaier, C.; Holten, D. *J. Am. Chem. Soc.* **1989**, *111*, 6500. (b) Fujitsuka, M.; Ito, O. In *Encyclopedia of Nanoscience and Nanotechnology*; Nalwa, H. S., Ed.; American Science Publishers: Stevenson Ranch, CA, 2004; Vol. 0.8, pp 593−615.

JP805352Y